# Ultrahydrophobic Surfaces. Effects of Topography Length Scales on Wettability

Didem Öner and Thomas J. McCarthy*

*Polymer Science and Engineering Department, University of Massachusetts, Amherst, Massachusetts 01003*

*Received April 20, 2000. In Final Form: June 23, 2000*

We discuss dynamic hydrophobicity from the perspective of the force required to move a water droplet on a surface and argue that the structure of the three-phase contact line is important. We studied the wettability of a series of silicon surfaces that were prepared by photolithography and hydrophobized using silanization reagents. Hydrocarbon, siloxane, and fluorocarbon surfaces were prepared. The surfaces contain posts of different sizes, shapes, and separations. Surfaces containing square posts with $X-Y$ dimensions of 32 $\mu$m and less exhibited ultrahydrophobic behavior with high advancing and receding water contact angles. Water droplets moved very easily on these surfaces and rolled off of slightly tilted surfaces. Contact angles were independent of the post height from 20 to 140 $\mu$m and independent of surface chemistry. Water droplets were pinned on surfaces containing square posts with larger dimensions. Increasing the distance between posts and changing the shape of the posts from square to staggered rhombus, star, or indented square caused increases in receding contact angles. We ascribe these contact angle increases to decreases in the contact length and increases in tortuosity of the three-phase contact line. The maximum length scale of roughness that imparts ultrahydrophobicity is ~32 $\mu$m.

## Introduction

The wettability of solid surfaces is an important property that is manipulated in numerous practical applications and, as well, is used as an analytical technique (contact angle analysis) to characterize surfaces in basic materials research. There is an enormous literature[1] that describes research over the past ~60 years that has been directed at studying and/or controlling the interaction between fluids (for the most part water) and solids. In many senses this mature field of science is well understood and is not controversial.

In this paper we are concerned with hydrophobicity and begin with a general discussion of this effect. Figure 1 shows a schematic representation of droplets of water on two different surfaces and asks the question, "Which surface is more hydrophobic?" Almost everyone would agree that the surface on the left is more hydrophobic than the one on the right; the contact angle is higher in the left case. The situation may, however, be more complex. What if when the surface on the right is tilted 1° from the horizontal, the droplet slides off, and when the surface on the left is tilted to any angle—even upside down—the droplet stays pinned to the surface? With these facts known we must say that the surface on the right is more hydrophobic. This is not just semantics; this issue has practical importance. In a static situation, clearly the left surface is more hydrophobic, but if you want a water-repellant surface, the static contact angle is irrelevant; you want the drop to move with very little applied force. Thus, dynamic wettability, which is a function of contact angle hysteresis and not the contact angle, is important.

The importance of contact angle hysteresis to hydrophobicity was first addressed decades ago, and the relationship shown in eq 1 was derived and reported.[2]

$$mg(\sin \alpha)/w = \gamma_{LV}(\cos \theta_R - \cos \theta_A) \qquad (1)$$

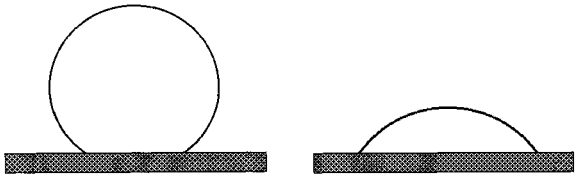

**Figure 1.** A schematic representation of water droplets on two surfaces. Which surface is more hydrophobic?

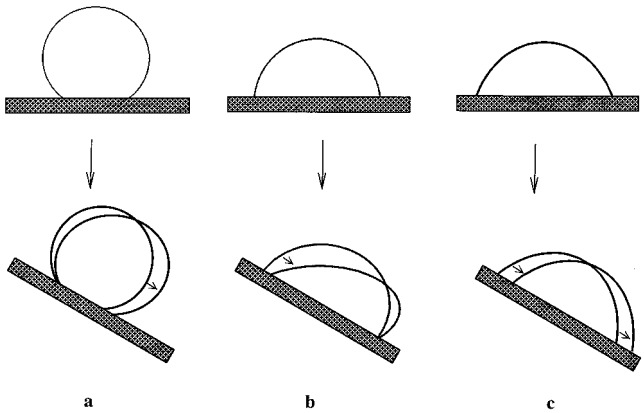


**Figure 2.** Water droplets behave differently on tilted surfaces because of the contact angle and contact angle hysteresis.

The equation predicts the minimum angle of tilt ($\alpha$) at which a droplet (with surface tension $\gamma_{LV}$) will spontaneously move, where $\theta_A$ and $\theta_R$ are the advancing and receding contact angles, $g$ is the force due to gravity, and $m$ and $w$ are the mass and width (horizontal to the direction of drop movement) of the droplet. It is clear from this equation that the *difference* between advancing and receding contact angles (hysteresis) and *not the absolute values* of the contact angles is important to hydrophobicity. That this is indeed the case is intuitive from the argument depicted in Figure 2. Consider three droplets of water on three surfaces. The surfaces in cases a and b exhibit water contact angles of $\theta_A/\theta_R = 120°/80°$, and the surface in case

* To whom correspondence should be addressed. E-mail: tmccarthy@polysci.umass.edu.

(1) Mittal, K. L., Ed. *Contact Angle, Wettability and Adhesion*; VSP: Utrecht, The Netherlands, 1993.

(2) Furmidge, C. G. L. *J. Colloid Sci.* **1962**, *17*, 309.

10.1021/la000598o CCC: $19.00 
Published on Web 08/26/2000

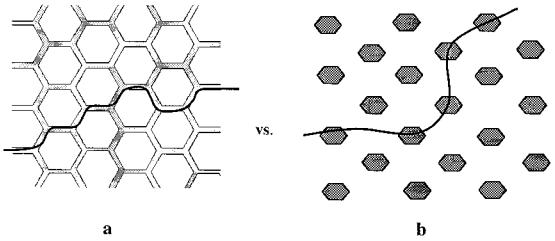


**Figure 3.** 2-Dimensional ($X-Y$) representations of two surfaces with the same $f_1$ and $f_2$ values, but very different contact line structures. The dark lines are meant to represent possible contact lines.

c exhibits $\theta_A/\theta_R = 70°/70°$. In case a, a 5 $\mu$L droplet was increased in volume to 10 $\mu$L; thus, it intersects the surface at its advancing angle. In case b, a 15 $\mu$L droplet was decreased in volume to 10 $\mu$L; thus, it intersects the surface at its receding angle. In case c, the 10 $\mu$L droplet is in equilibrium with $\theta_A/\theta_R = 70°/70°$. When the surfaces are tilted, different events happen with each droplet. On surface a, the downhill side of the droplet can advance, but the uphill side stays pinned until the receding angle is reached. This 2-dimensional representation oversimplifies the situation. There is a barrier to advancing due to the change in shape of the droplet; the volume stays constant but the air−water interfacial area increases. On surface b, the uphill side of the droplet can recede, but the downhill side stays pinned until the advancing angle is reached. Again there is a barrier to receding due to the change in shape of the droplet. On surface c, the droplet can advance and recede simultaneously with no change in the droplet shape.

This discussion, thus far, offers little new insight into wettability or hydrophobicity as these issues were discussed (in some form) in the literature decades ago,[2,3−9] but it is apparently necessary as indicated by numerous recent reports[10−19] of surfaces described as "super water repellant", "ultrahydrophobic", and "ultra water repellant" that report only one contact angle.

Another issue that is of practical importance on real surfaces is the three-phase (solid−liquid−air) contact line structure (shape, length, continuity of contact, amount of contact; these are both topological and topographical concerns). When liquid moves in contact with a surface, for instance water moving through a pipe, the velocity at the surface is 0. This is the no-slip boundary condition of fluid mechanics.[20] Therefore, when a droplet moves on a surface, the only solid−liquid interfacial water molecules that move are those on the contact line. On most materials, a droplet placed on the surface will come to rest at a local energy minimum (due to either chemical structure or topography), the contact line will be fixed, and there will be energy barriers for advancing and receding; these are the causes of hysteresis. We recently[21,22] described two approaches to destabilizing the contact line. One involves preparing randomly rough hydrophobic surfaces by various techniques that form contorted discontinuous contact lines with water droplets. The other involves preparing smooth surfaces with flexible, liquidlike covalently at-

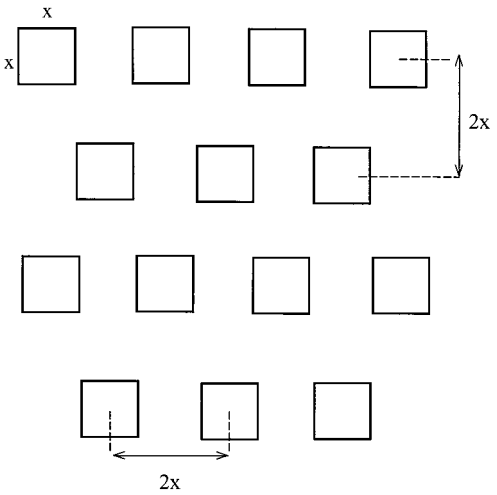


**Figure 4.** 2-Dimensional ($X-Y$) representation of a series of silicon surfaces containing hexagonally arrayed square posts, $X = 2$, 8, 16, 32, and 128 $\mu$m. Surfaces with post heights ($Z$) of 20, 40, 60, 80, 100, and 140 $\mu$m were prepared.

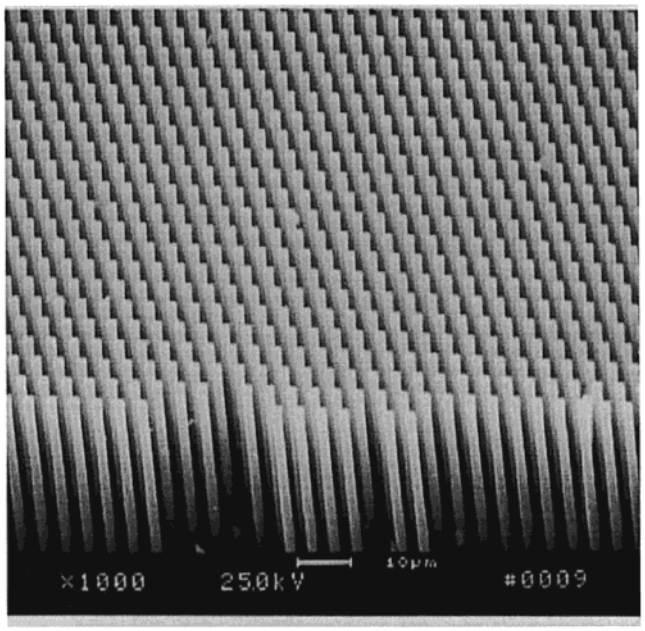


**Figure 5.** Representative SEM image of a surface described in Figure 4. This surface contains 2 $\mu$m × 2 $\mu$m × 100 $\mu$m square posts.

(3) Shuttleworth, R.; Bailey, G. L. *Discuss. Faraday Soc.* **1948**, *3*, 16.
(4) Bikerman, J. J. *J. Phys. Chem*, **1950**, *54*, 653.
(5) Good, R. J. *J. Am. Chem. Soc.* **1952**, *74*, 504.
(6) Schwartz, A. M.; Minor, F. W. *J. Colloid Sci.* **1959**, *14*, 584.
(7) Johnson, R. E., Jr.; Dettre, R. H. *Adv. Chem. Ser.* **1963**, *43*, 112.
(8) Dettre, R. H.; Johnson, R. E. *Wetting*; SCI Monograph No. 25; Society of Chemical Industry; London, 1967; p 144.
(9) Wolfram, E.; Faust, R. In *Wetting, Spreading and Adhesion*, Padday, J. F., Ed.; Academic Press: London, 1978; p 213.
(10) Onda, T. Shibuichi, S.; Satoh, N.; Tsujii, K. *Langmuir* **1996**, *12*, 2125.
(11) Shibuichi, S.; Onda, T.; Satoh, N.; Tsujii, K. *J. Phys. Chem.* **1996**, *100*, 19512.
(12) Tadanaga, K.; Katata, N.; Minami, T. *J. Am. Ceram. Soc.* **1997**, *80*, 1040.
(13) Tadanaga, K.; Katata, N.; Minami, T. *J. Am. Ceram. Soc.* **1997**, *80*, 3213.
(14) Veeramasuneni, S.; Drelich, J.; Miller, J. D.; Yamauchi, G. *Prog. Org. Coat.* **1997**, *31*, 265.
(15) Ogawa, K.; Soga, M.; Takada, Y.; Nakayama, I. *Jpn. J. Appl. Phys., Part 2* **1993**, *32*, L614.
(16) Kunugi, Y.; Nonaku, T.; Chong, Y. B.; Watanabe, N. *J. Electroanal. Chem.* **1993**, *353*, 209.
(17) Schakenraad, J. M.; Stokroos, I.; Bartels, H.; Busscher, H. J. *Cells Mater.* **1992**, *2*, 193.
(18) Hozumi, A.; Takai, O. *Thin Solid Films* **1997**, *303*, 222.
(19) Miller, J. D.; Veeramasuneni, S.; Drelich, J.; Yalamanchili, M. R.; Yamauchi, Y. *Polym. Eng. Sci.* **1996**, *36*, 1849.
(20) Bird, R. B.; Stewart, W. E.; Lightfoot, E. N. *Transport Phenomena*; Wiley: New York, 1960; p 37.
(21) Chen, W.; Fadeev, A. Y.; Hsieh, M. C.; Öner, D.; Youngblood, J. P.; McCarthy, T. J. *Langmuir* **1999**, *15*, 3395.
(22) Youngblood, J. P.; McCarthy, T. J. *Macromolecules* **1999**, *32*, 6800.

**Table 1. Water Contact Angle Data for Silane-Modified Hexagonally Arrayed 40 $\mu$m High Square Post Surfaces Described in Figures 4 and 5**

| silicon surface | DMDCS-modified | | ODMCS-modified | | FDDCS-modified | |
|---|---|---|---|---|---|---|
| | $\theta_A$ (deg) | $\theta_R$ (deg) | $\theta_A$ (deg) | $\theta_R$ (deg) | $\theta_A$ (deg) | $\theta_R$ (deg) |
| smooth | 107 | 102 | 102 | 94 | 119 | 110 |
| $^{2\mu m}SP^{40\mu m}$ | 176 | 141 | 174 | 141 | 170 | 146 |
| $^{8\mu m}SP^{40\mu m}$ | 173 | 134 | 173 | 139 | 170 | 140 |
| $^{16\mu m}SP^{40\mu m}$ | 171 | 144 | 174 | 134 | 168 | 145 |
| $^{32\mu m}SP^{40\mu m}$ | 168 | 142 | 170 | 132 | 170 | 146 |
| $^{64\mu m}SP^{40\mu m}$ | 139 | 81 | 114 | 65 | 149 | 100 |
| $^{128\mu m}SP^{40\mu m}$ | 116 | 80 | 95 | 58 | 131 | 93 |

**Table 2. Water Contact Angle Data for ODMCS−Modified Surfaces Containing 16 $\mu$m × 16 $\mu$m and 32 $\mu$m × 32 $\mu$m Square Posts of Different Heights**

| silicon surface | post height ($\mu$m) | $\theta_A$ (deg) | $\theta_R$ (deg) |
|---|---|---|---|
| $^{16\,\mu m}SP^{20\mu m}$ | 20 | 173 | 138 |
| $^{16\,\mu m}SP^{40\mu m}$ | 40 | 174 | 134 |
| $^{16\,\mu m}SP^{60\mu m}$ | 60 | 169 | 138 |
| $^{16\,\mu m}SP^{80\mu m}$ | 80 | 169 | 136 |
| $^{16\,\mu m}SP^{100\mu m}$ | 100 | 173 | 138 |
| $^{16\,\mu m}SP^{140\mu m}$ | 140 | 168 | 136 |
| $^{32\,\mu m}SP^{20\mu m}$ | 20 | 170 | 137 |
| $^{32\,\mu m}SP^{40\mu m}$ | 40 | 170 | 132 |
| $^{32\,\mu m}SP^{60\mu m}$ | 60 | 168 | 139 |
| $^{32\,\mu m}SP^{80\mu m}$ | 80 | 167 | 134 |
| $^{32\,\mu m}SP^{100\mu m}$ | 100 | 173 | 134 |
| $^{32\,\mu m}SP^{140\mu m}$ | 140 | 166 | 131 |

tached monolayers. Rotating groups on these surfaces move the contact line. In both cases the contact line is unstable; thus, the droplet is constantly advancing and receding at different contact line points. Droplets do not come to rest on these surfaces, or they move very easily.

One of the objectives of the work reported in this paper is to resolve the issue of the size scale of roughness needed to impart ultrahydrophobicity. The more recent reports of anomalously high contact angles[10−19] have indicated that micrometer-, submicrometer, and nanometer-scale roughness imparts this property. Older reports[8,23,24] from the 1940s, 1950s, and 1960s and wettability data on natural water-repellant surfaces,[25] however, suggest that much larger features (tens to hundreds of micrometers) can also function in this manner. It is not clear from the literature whether the surfaces with high length scale roughness also have lower length scale topographies superimposed on the larger features. We have prepared a series of silicon oxide surfaces by photolithography that have roughness on different length scales, hydrophobized these surfaces using reactive silane chemistry, and measured the wettability using dynamic contact angle analysis. A recent report by Bico et al.[26] describes the wettability of three surfaces, one of which is similar to some of those reported here.

## Experimental Section

**General Procedures.** Ethanol, toluene, sulfuric acid, and hydrogen peroxide (30%) were used as received from Fisher. Organosilanes were obtained from Gelest and used as received. House-purified water (reverse osmosis) was further purified using a Millipore Milli-Q system that involves reverse osmosis, ion exchange, and filtration steps ($10^{18}$ Ω/cm). Contact angle measurements were made using a Ramé-Hart telescopic goniometer with a 24-gauge flat-tipped needle; dynamic advancing and receding angles were recorded as the probe fluid, water, purified as described above, was added to and withdrawn from the drop, respectively. The values reported are averages of greater than eight measurements made on different areas of the sample surface. The modified surfaces exhibited very homogeneous surfaces as evidenced by the contact angle, and all measurements for all surfaces were within ±2° of the averages. Scanning electron micrographs were obtained using an Amray 1803TC instrument with an accelerating voltage of 25 kV.

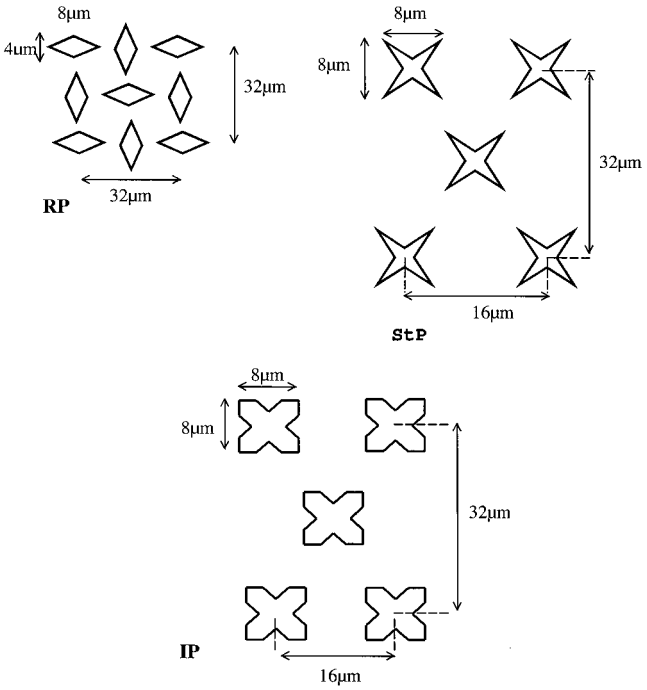


**Figure 6.** 2-Dimensional ($X-Y$) representations of surfaces containing different geometry posts: RP, staggered rhombus posts; StP, four-armed star-shaped posts; IP, indented square posts.

**Preparation of Silicon Substrates.** Silicon wafers (4 and 3 in.) were obtained from the International Wafer Service (⟨100⟩ orientation, P/B-doped, resistivity from 20 to 40 Ω cm, thickness from 450 to 575 $\mu$m). A contact lithographic mask (with hexagonally arrayed square posts of 16, 32, 64, and 128 $\mu$m length and width) was constructed by Photronics Inc. The other masks were designed using a CAD program and prepared with a GCA PG3600F optical pattern generator. Photolithography was used to transfer the patterns of the masks onto the silicon wafers. After irradiation, the wafers were etched using a Plasma Therm SLR-770 for different durations. When the etching process was complete, the wafers were cleaned using a Branson IPC P2000 Barrel Etcher. Wafers were then placed in a solution of ammonium hydroxide, hydrogen peroxide, and water (4:1:1) for 15 min, rinsed with copious amounts of water, and spin dried. The wafers were then cut into 1.5 × 1.5 cm pieces, placed in a custom-designed (slotted hollow glass cylinder) sample holder, and cleaned by submersion into a mixture of concentrated sulfuric acid and hydrogen peroxide (30%) (7:3) overnight. The wafers were then rinsed with copious amounts of purified water and dried in a clean oven at 120 °C for 2 h immediately prior to silanization reactions.

**Reaction of Silicon Substrates with Organosilanes.** The silicon substrates were placed in a custom-designed (slotted hollow glass cylinder) sample holder, which was then placed in a flask containing 0.5 mL of organosilane reagent: dimethyldichlorosilane (DMDCS), *n*-octyldimethylchlorosilane (ODMCS), or heptadecafluoro-1,1,2,2-tetrahydrodecyldimethylchlorosilane (FDDCS). The wafers were not in contact with the liquid silanes. The vapor-phase reactions were carried out for 3 days at 65−70 °C. The hydrophobized wafers were rinsed with toluene (two aliquots), ethanol (three aliquots), 1:1 ethanol/water (two aliquots), water (two aliquots), ethanol (two aliquots), and then water (three aliquots) and were then dried in a clean oven at 120 °C for 30 min.

(23) Cassie, A. B. D.; Baxter, S. *Trans. Faraday Soc.* **1944**, *40*, 546.
(24) Bartell, F. E.; Shepard, J. W. *J. Phys. Chem.* **1953**, *57*, 211.
(25) Meinhuis, C.; Barthlott, W. *Ann. Bot. (London)* **1997**, *79*, 667.
(26) Bico, J.; Marzolin, C.; Quéré, D. *Europhys. Lett.* **1999**, *47*, 220.

## Results and Discussion

We have discussed in two publications,[21,22] why surfaces containing hydrophobic posts should form discontinuous and unstable three-phase contact lines with water droplets. The posts must be close enough together and hydrophobic enough that water does not intrude between them. Surfaces such as these are referred to as composite surfaces as the intersection of the water droplet with the surface consists of a composite mixture of water−solid interface area and water−air interface area. The wettability of such surfaces was first addressed by Cassie,[22] and eq 2 was derived that relates the contact angle of a

$$\cos \theta_C = f_1 \cos \theta - f_2 \qquad (2)$$

liquid on a composite (air−solid mixture) surface ($\theta_C$) to the contact angle on a smooth surface of the same solid ($\theta$) and the fraction of water−solid interface area ($f_1$) and water−air interface area ($f_2$), $f_1 + f_2 = 1$. We stress that this equation is derived for a drop at equilibrium on a surface; thus, the contact angles predicted are "equilibrium contact angles". We argue above that the structure of the three-phase contact line is important to dynamic wettability ($\theta_A$, $\theta_R$, and hysteresis), and Cassie's analysis does not take the three-phase contact line structure into account. Surfaces with many different topographies can have the same $f_1$ and $f_2$ values, but can have very different contact line structures. Figure 3 shows representations of two surfaces with the same $f_1$ and $f_2$ values. Cassie's equation predicts the same equilibrium contact angles, but the advancing and receding contact angles will be very different on these surfaces because, in case a, a nearly continuous contact line can form (pinning the drop), but in case b, the contact line is discontinuous and unstable.

Figure 4 is a 2-dimensional schematic representation of one series of silicon oxide surfaces that was prepared using photolithographic techniques. These surfaces are hexagonally arrayed square posts varying in size from 2 $\mu$m × 2 $\mu$m to 128 $\mu$m × 128 $\mu$m. Different post heights (20, 40, 60, 80, 100, and 140 $\mu$m) were prepared by varying the etching time for two different size posts. The posts are spaced as indicated in the figure. Figure 5 is a representative scanning electron microscopy (SEM) image of one of the surfaces (2 $\mu$m × 2 $\mu$m × 100 $\mu$m posts). These surfaces were oxidatively cleaned (to remove any of the lithography mask and/or etching chemicals) and chemically modified by reaction with silanization reagents in the vapor phase. Reaction conditions were chosen to give dense monolayers.[27]

Table 1 shows water contact angle data for surfaces that were etched to give 40 $\mu$m high posts and reacted with DMDCS, ODMCS, or FDDCS. Data for smooth silicon/silicon oxide surfaces are shown for comparison. The surfaces are named $^{X}SP^{Y}$, with the superscript $X$ indicating the post length and width and the superscript $Y$ indicating the post height. The surfaces with post sizes of 32 $\mu$m and less exhibit both high advancing and high receding contact angles. We ascribe the slight differences in contact angles between the differently modified surfaces to experimental error in the modification reactions or in the measurement of contact angles and not to the size of the posts or the identity of the silanization reagents. All of these surfaces are extremely hydrophobic. Water droplets were unstable on these surfaces and were observed to be constantly rotating while at rest on stable horizontal surfaces. Droplets moved spontaneously on slightly tilted surfaces. For the surfaces with post sizes of 64 $\mu$m and greater, low receding contact angles (lower than those on the smooth surfaces) were observed. Advancing angles were higher than those on the smooth surfaces, but lower than those on the surfaces with smaller features. Water drops are pinned on these surfaces and do not rotate or move spontaneously when the surfaces are slightly tilted. It is apparent that water intrudes between the greater spaced posts and that the contact line is pinned by the greater solid−liquid contact. We note that all of these surfaces contain 25% solid−liquid interfacial area ($f_1$ in eq 2); this equation predicts equilibrium contact angles (using the measured advancing

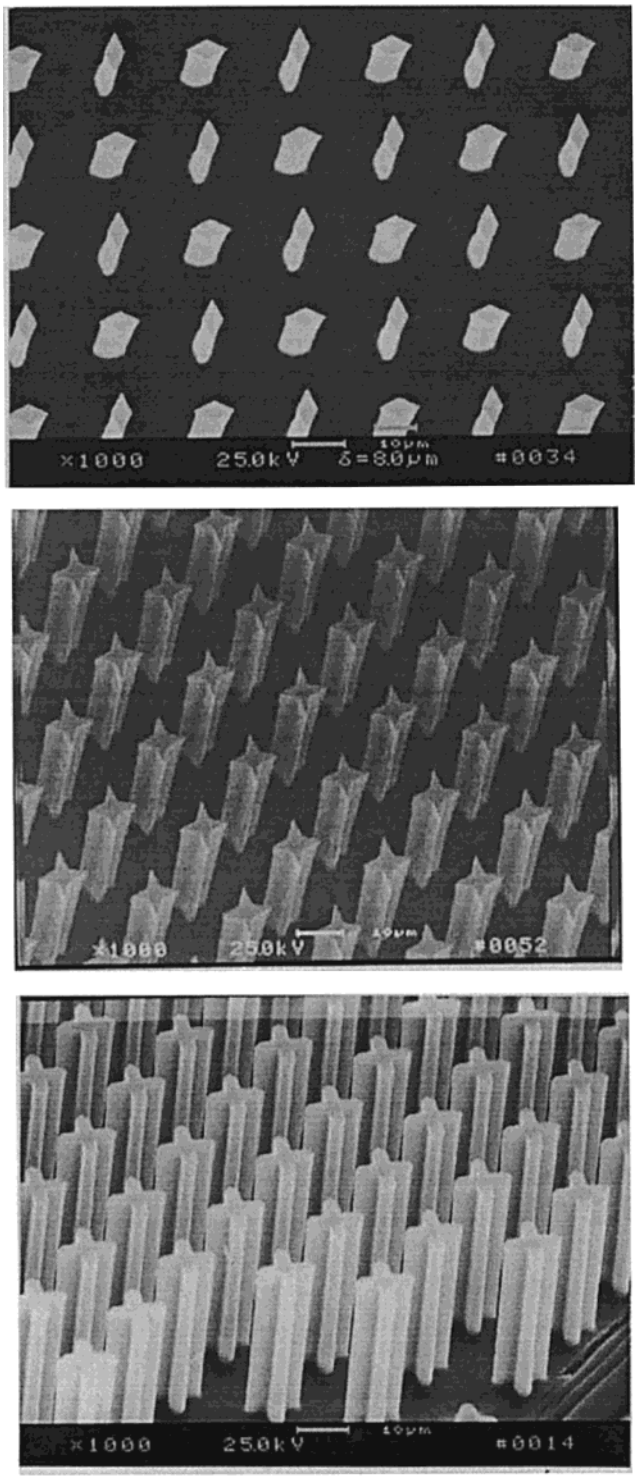


**Figure 7.** SEM images of the surfaces described in Figure 6.

(27) Fadeev, A. Y.; McCarthy, T. J. *Langmuir* **1999**, *15*, 3759.

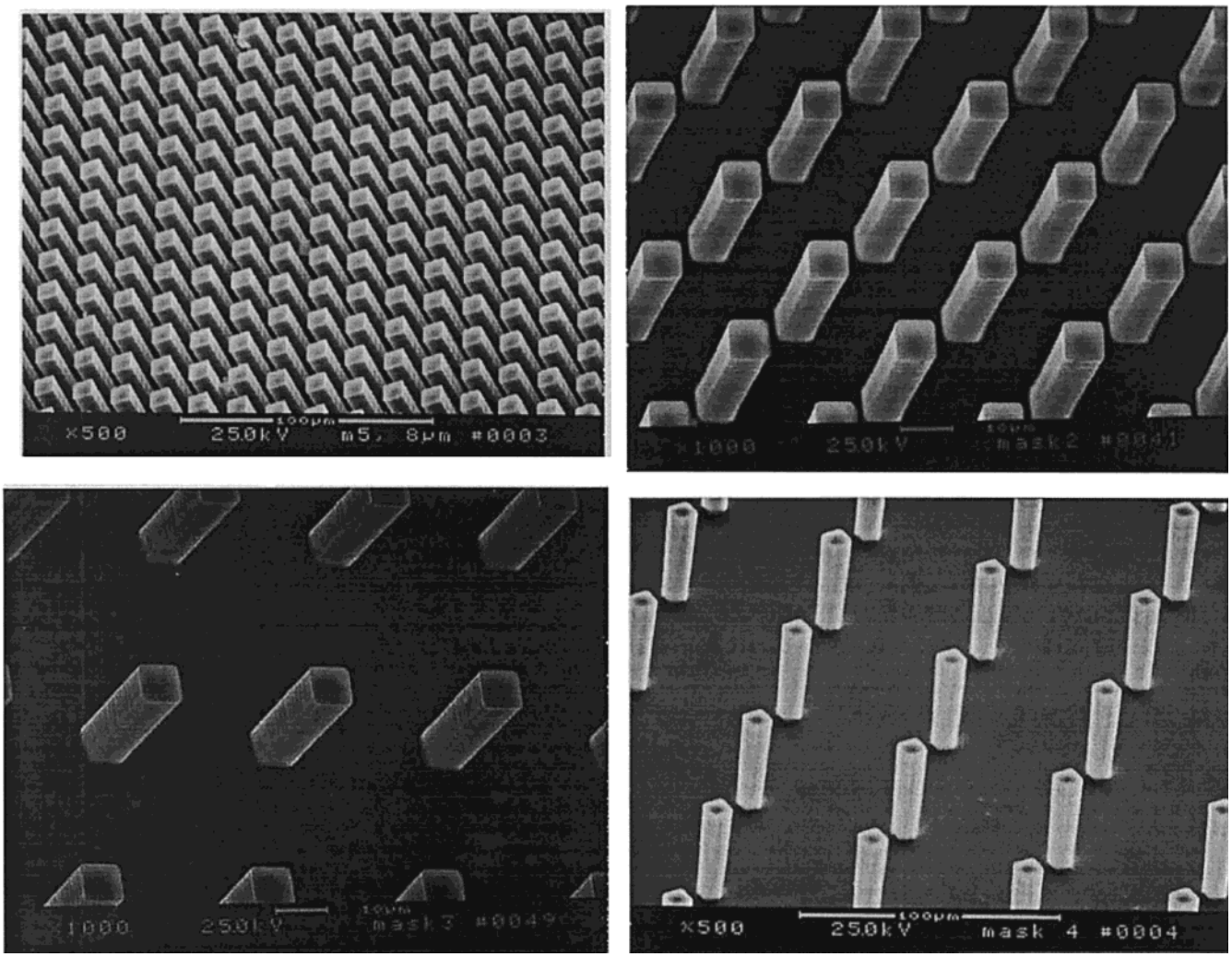


**Figure 8.** SEM images of surfaces containing 8 $\mu$m × 8 $\mu$m square posts with different spacings.

contact angles on smooth surfaces) of 145°, 143°, and 150° for the DMDCS, ODMCS, and FDDCS surfaces, respectively. These are in line (between the measured advancing and receding contact angles) with the surfaces containing features of 32 $\mu$m and less.

Surfaces containing 16 and 32 $\mu$m posts with post heights varying from 20 to 140 $\mu$m were prepared and derivatized using ODMCS. Contact angles were measured and are reported in Table 2. The contact angles are independent of the height of the posts, indicating that water does not intrude between them (the probe fluid cannot detect the depth of the region that it does not penetrate).

The surfaces described thus far (square posts) with features of 32 $\mu$m and smaller exhibit very high advancing and receding contact angles, but significant (30−40°) hysteresis. Water droplets come to rest on these surfaces when the surfaces are horizontal (but rotate continuously). This behavior differs from the randomly rough surfaces that we have prepared[21,22] on which droplets move spontaneously on horizontal surfaces. We suspect that the regular hexagonal array of features with regions that can support a straight contact line over significant lengths is the source of this hysteresis. We designed and prepared three different surfaces with the objective of contorting the three-phase contact line. These are described in Figure 6, and SEM images are shown in Figure 7. These surfaces are named RP for the staggered rhombus-shaped posts, IP for the indented square-shaped posts, and StP for the four-point star-shaped posts. The post height of these surfaces was maintained at 40 $\mu$m. We also prepared a series of surfaces containing 8 $\mu$m × 8 $\mu$m hexagonally arrayed square posts (40 $\mu$m high) that were spaced at greater distances than the surfaces described in Figures 4 and 5. SEM images of these are shown in Figure 8. These were prepared with the objective of making the three-phase contact line less continuous.

**Table 3. Water Contact Angle Data for Silane-Modified Surfaces Containing Differently Shaped Posts and 8 $\mu$m × 8 $\mu$m Square Posts Spaced at Various Distances (Described in Figures 7 and 8)**

| silicon surface | DMDCS | | ODMCS | | FDDCS | |
|---|---|---|---|---|---|---|
| | $\theta_A$ (deg) | $\theta_R$ (deg) | $\theta_A$ (deg) | $\theta_R$ (deg) | $\theta_A$ (deg) | $\theta_R$ (deg) |
| $RP^{40\mu m}$ | 176 | 156 | 174 | 155 | 168 | 153 |
| $IP^{40\mu m}$ | 175 | 143 | 173 | 140 | 169 | 146 |
| $StP^{40\mu m}$ | 175 | 149 | 174 | 147 | 170 | 148 |
| $_{16\mu m}SP^{40\mu m}$ | 173 | 134 | 173 | 139 | 170 | 140 |
| $_{23\mu m}SP^{40\mu m}$ | 175 | 146 | 172 | 147 | 167 | 147 |
| $_{32\mu m}SP^{40\mu m}$ | 173 | 154 | 172 | 154 | 169 | 155 |
| $_{56\mu m}SP^{40\mu m}$ | 121 | 67 | 112 | 68 | 134 | 92 |

Water contact angle data for the silane-modified surfaces shown in Figures 7 and 8 are reported in Table 3. The subscripts in the structure names indicate the minimum distance between post centers. The entry labeled $_{16\mu m}SP^{40\mu m}$ is the same surface as that labeled $^{8\mu m}SP^{40\mu m}$ in Table 1 and is displayed there for comparison (these squares are spaced by 16 $\mu$m). Changing the shape of the posts from square to indented square, star, or staggered

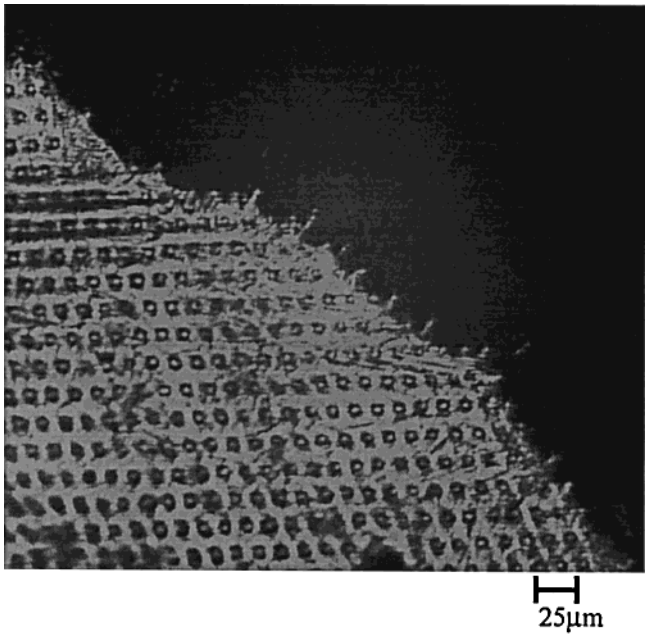


**Figure 9.** Optical micrograph of the (solidified) three-phase contact line of molten Woods metal on $_{32\mu m}SP^{40\mu m}$.

rhombus does not affect the advancing contact angles, but causes significant increases (up to 22°) in receding contact angles (and corresponding decreases in hysteresis). The receding contact angles are higher for the staggered rhombus posts than those for the star-shaped posts, which are higher than those for the indented square posts. We interpret these changes as due to more contorted and longer three-phase contact lines. Increasing the spacing between the posts also results in no changes in the advancing contact angles and increases in the receding contact angles (up to 20°) for square posts spaced up to 32 $\mu$m. We interpret these increases as due to decreases in the contact length of three-phase contact lines. Contact angles decreased significantly for the sample with posts spaced by 56 $\mu$m. Water intrudes between these posts, increasing the contact length of the three-phase contact line.

We attempted to view the three-phase contact line between water and the surfaces reported here using optical microscopy—with no success. The droplets acted as lenses, and we could not focus on the contact lines. To overcome this problem, we put drops of molten Woods metal on the surfaces and viewed the contact lines after the metal solidified and was removed from the surfaces. Figure 9 shows an optical micrograph of the Woods metal−silicon−air three-phase contact line on the surface named $_{32\mu m}SP^{40\mu m}$ in Table 3. The contact line is clearly contorted by the square posts on the surface.

Although the surfaces reported here are extremely hydrophobic, they are not as hydrophobic as many of the surfaces that we have prepared that contain random roughness (perhaps at multiple length scales).[21,22] We believe that this is due to two effects: First, on the surfaces reported here, that were prepared by photolithography and etching, the three-phase contact line is tortuous only in the $X-Y$ plane of the surface (all of the posts are the same height). Contact lines on randomly rough surfaces are tortuous in 3 dimensions; thus, the contact lines can be longer and less stable. Second, these lithographed surfaces are very regular, and the contact line can register with the posts in metastable geometries that will differ around the perimeter of the drop as a function of the angle between the contact line and the hexagonal spacing direction. We predict that surfaces with randomly arrayed posts of different heights will be even more hydrophobic than those reported here.

## Summary

The wettability of a number of patterned silicon surfaces that were prepared by photolithography and hydrophobized using silanization chemistry was determined. Surfaces containing square posts with $X-Y$ dimensions of 2 and 32 $\mu$m and similar distances between the posts exhibited ultrahydrophobic behavior with high advancing and receding water contact angles. Water droplets moved very easily on these surfaces and rolled off of slightly tilted surfaces. Contact angles were independent of the post height from 20 to 140 $\mu$m and independent of surface chemistry (siloxane-, hydrocarbon-, and fluorocarbon-modified surfaces were prepared). Surfaces containing square posts with $X-Y$ dimensions of 64 and 128 $\mu$m with similar distances between them were not ultrahydrophobic; water droplets were pinned on these surfaces, and water apparently intruded between the posts. Increasing the distance between posts caused increases in receding contact angles up to the point that water intruded between the posts. This is due to decreases in the contact length of the three-phase contact line. Changing the shape of the posts from square to staggered rhombus, star, or indented square also increased the receding angles due to the more contorted contact lines that form on these surfaces. The maximum length scale of roughness that imparts ultrahydrophobicity is ~32 $\mu$m for surfaces consisting of square posts.

**Acknowledgment.** We thank the University of Massachusetts Materials Research Science and Engineering Center and the Office of Naval Research for financial support. This work was performed in part at the Cornell Nanofabrication Facility, which is supported by the National Science Foundation under Grant ECS 973123, its users, Cornell University, and Industrial Affiliates.

LA000598O